In-situ characterization of heterogeneous catalysts using time-resolved X-ray diffraction

José A. Rodriguez and Jonathan C. Hanson

Chemistry Department. Brookhaven National Laboratory. Upton, NY 11973, USA

Abstract

Time-resolved x-ray diffraction (XRD) has emerged as a powerful technique for studying the behavior of heterogeneous catalysts (metal oxides, sulfides, carbides, phosphides, zeolites, etc) *in-situ* during reaction conditions. The technique can identify the active phase of a heterogeneous catalyst and how its structure changes after interacting with the reactants and products (80 K < T < 1200 K; P< 50 atm). In this article, we review a series of recent works that use time-resolved XRD for studying the reduction/activation of oxide catalysts (CuO, Cu_2O, CuO/CeO_2, $Ce_{1-x}Cu_xO_2$, NiO, $NiMoO_4$, $CoMoO_4$). These studies illustrate the important role played by O vacancies in the mechanism for reduction of an oxide. The phenomenological kinetic models frequently used in the description of the reduction process can be useful, but a more relevant aspect is the initial production of active sites for the rapid dissociation of H_2. This alone can lead to the appearance of "induction periods" in the reaction kinetics and the possibility for autocatalysis. *In-situ* studies for the water-gas shift reaction on CuO, Cu_2O, CuO/CeO_2 and $Ce_{1-x}Cu_xO_2$ catalysts show that Cu^0 is the active species of copper (i.e. no Cu^{+1} or Cu^{+2} cations), but interactions with the oxide support are necessary in order to obtain high catalytic activity.

Palabras clave: Catalisis; catyalizadores de óxido de cobre; difración de rayos-X; reacción de "water-gas shift".

Caracterización *in-situ* de catalizadores heterogeneos utilizando difracción de rayos X con resolución en el tiempo

Resumen

La difraccion de rayos X con resolucion en el tiempo se ha convertido en una tecnica muy versatil para estudiar el comportamiento de catalizadores heterogeneos (oxidos, sulfuros, carburos, fosfuros, zeolitas, etc) *in-situ* durante el proceso de conversion de los reactantes. Esta tecnica es capaz de identificar las fases activas de un catalizador heterogeneo y como su estructura cambia cuando interacciona con reactantes y productos en un amplio rango de temperaturas y presiones (80 K < T < 1200 K; P< 50 atm). En este articulo se discuten una serie de trabajos donde la difraccion de rayos X con resolucion temporal ha sido aplicada para estudiar la reduccion de oxidos en hidrogeno y la reaccion de "water-gas shift" (CO + $H_2O \rightarrow CO_2$ + H_2) sobre

*   Autor para la correspondencia. E-mail: rodrigez@bnl.ge.ob

---

catalizadores de CuO, Cu_2O, CuO/CeO_2 y $Ce_{1-x}Cu_xO_2$. Estos estudios indican que Cu^0 es la fase active de cobre, esto es reduccion de cationes de Cu^{+1} o Cu^{+2} pero interacciones con ceria son necesarias para obtener alta actividad catalitica.

Key words: Catalysis cooper oxide; catalysts; X-ray; difraction water-gas shift reaction.

Introduction

The development of techniques for characterizing the structural properties of catalysts under the high-pressure conditions of industrial processes is widely recognized as a top priority in the area of heterogeneous catalysis. Under reaction conditions a catalyst can undergo chemical transformations that drastically modified its composition with respect to that obtained during the synthesis of the material. To optimize the performance of the catalyst, it is desirable to know what is its active phase. Investigations at Brookhaven National Laboratory have established the feasibility of conducting sub-minute, time-resolved *in situ* x-ray diffraction (XRD) experiments under a wide variety of temperature and pressure conditions (80 K < T < 1200 K; P< 50 atm) (1). This important advance results from combining the high intensity of synchrotron radiation with new parallel data-collection devices (1). Similar *in situ* diffraction facilities have also been established at the Daresbury synchrotron (2) and HASYLAB (3). Using time-resolved XRD, one can get information about (1):

Phase identification and composition of catalysts under reaction conditions

- Kinetics of crystallization of bulk solids and nanoparticles

- Crystallite size as a function of time/temperature

- Identify crystalline or amorphous intermediates during phase transitions occurring in bulk solids or nanoparticles

- Real-time crystal structure refinement

Examples of problems studied to date with time-resolved XRD and related to catalysis include (1,4-15):

- Hydrothermal synthesis of zeolites

- Hydrothermal conversion of zeolites

- Binding of substrates and inhibitors in zeolites

- Reduction/oxidation cycles in oxide catalysts

- Phase transformations in oxide catalysts for the partial oxidation

- of hydrocarbons and the water-gas shift reaction.

- Sulfidation of oxide precursors for HDS catalysts

- Regeneration of S-poisoned oxide catalysts

- Synthesis of metal phosphide catalysts

An early review article by Norby and Hanson (1) was focused on the applications of the technique in solid-state chemistry and materials science. In this article, we will review a series of recent works (9-15) that illustrate the power of time-resolved XRD for studying the behavior of oxide catalysts *in-situ* under reaction conditions. Metal oxides are used as catalysts in a large variety of commercial processes for the conversion of hydrocarbons, the roduction of hydrogen, and the synthesis of fine chemicals (16, 17). In addition, due to their low cost, metal oxides are also used as supports of many other catalytic materials (metals, sulfides, carbides, nitrides, etc) (1, 2).
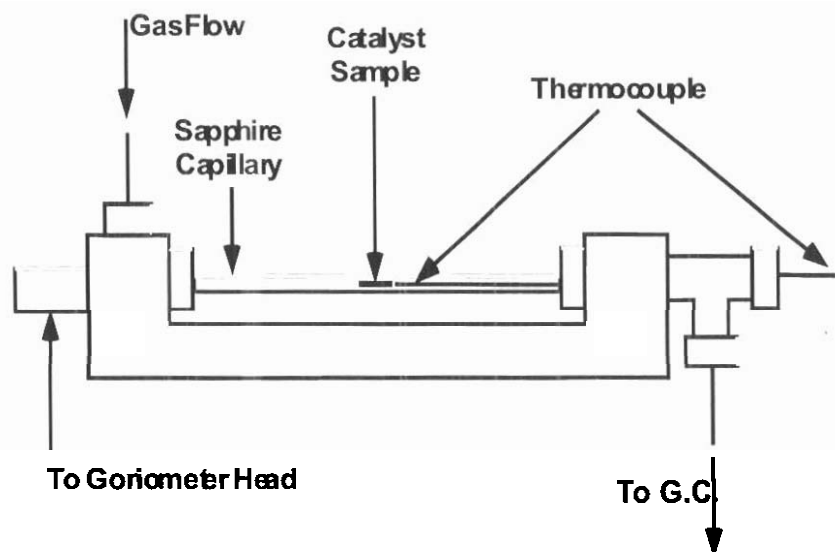
Figure 1.   Sapphire flow cell for *in-situ* time-resolved x-ray diffraction studies of catalysts (taken from ref. (18)).

Experimental

The time-resolved diffraction data were collected on beam line X7B of the National Synchrotron Light Source (NSLS) (1). The oxide samples were loaded into a sapphire capillary that was attached to a flow system (Figure 1) (18). A small resistance heater was wrapped around the capillary, and the temperature was monitored with a 0.1 mm chromel-alumel thermocouple that was placed in the capillary near the sample. The composition of the gas leaving the capillary could be determined by means of gas chromatography or mass spectrometry. A MAR345 detector was used to record full X-ray patterns, and the powder rings were first integrated with the FIT2D code (19). The FIT2D parameters for the integration of the data were obtained with a standard LaB_6 crystal compound. From the XRD data, occupancies of atoms, accurate lattice constants, and the concentration of phases appearing during reaction were determined by a Rietveld analysis using the GSAS (general structure analysis system) program (20).

Reduction/activation of metal oxides

The controlled synthesis of well-defined suboxides through reduction in H_2 is a key issue in the activation of oxide catalysts (16, 17). In practical terms, one needs to know what are the kinetic and thermodynamic parameters that determine the formation of a suboxide (17, 21). At a fundamental level, one must understand the interplay among H_2 dissociation, oxygen removal (i.e. generation of O vacancies), and the relative stability of a suboxide. Traditionally the reduction process has been described using phenomenological models where the rate of reaction depends on the initial nucleation of the new phase (i.e., the reduced oxide) or on the area of the reduced-phase/oxide interface (17, 21). Recent studies of time-resolved XRD illustrate the important role played by O vacancies in the mechanism for the reduction of an oxide (11). The phenomenological kinetic models frequently used in the description of the reduction process (17, 21) can be useful, but a more relevant aspect is the initial production of active sites for the rapid dissociation
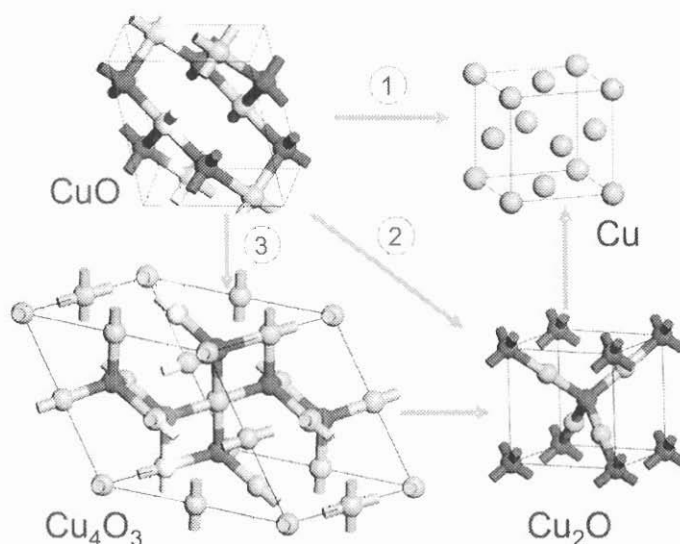
Figure 2. Three possible pathways for the transformation of CuO to Cu.

of H_2 (11). This alone can lead to the appearance of "induction periods" in the reaction kinetics and the possibility for autocatalysis. In some cases, the situation can become even more complex due to the embedding of hydrogen into the lattice of the oxide before the reduction process starts (10, 11).

Copper oxide, an antiferroelectric semiconductor with a band gap of about 1.4 eV, is a benchmark system which can undergo a sequential reduction for a change in oxidation state from "+2" to 0 (CuO → Cu_4O_3 → Cu_2O → Cu). Three possible pathways for the transformation of CuO to Cu are displayed in Figure 2, including a direct reduction (CuO→Cu, pathway 1), or reduction mechanisms that involve either one intermediate (CuO→Cu_2O→Cu, pathway 2) or two intermediates (CuO→Cu_4O_3→Cu_2O→Cu, pathway 3). CuO, Cu_4O_3 and Cu_2O are well known copper oxides with monoclinic, tetragonal and cubic crystal structures, respectively (22). CuO is used as a catalyst or catalyst precursor in many chemical reactions that involve hydrogen as a reactant or a product: methanol synthesis from CO (CO + $2H_2$ → CH_3OH) or CO_2 (CO_2 + $3H_2$ → CH_3OH + H_2O), the water-gas shift reaction (CO +

H_2O → CO_2 + H_2), methanol steam reforming (CH_3OH + H_2O → CO_2 + $3H_2$), oxidative methanol reforming (CH_3OH + ¼ O_2 + ½ H_2O → CO_2 + 5/2 H_2), NO reduction (NO + H_2 → ½ N_2 + H_2O), etc (16, 17). For years, there has been a big controversy about the relative importance of Cu^{1+} and Cu^0 centers in several of these catalytic reactions (23, 24, 25). The data reported in the literature do not agree in the mechanism for CuO reduction (22-24). Experiments of H_2-temperature programmed reduction (TPR) show that the reduction of CuO occurs in one, two or even three steps. These discrepancies could be a consequence of the different conditions used in the reduction experiments, or they could originate from differences in the handling/ preparation of the CuO samples. To solve these issues, we investigated the reaction of H_2 with Cu_2O, CuO and $Ce_{1-x}Cu_xO_2$ *in-situ* using time-resolved XRD and x-ray absorption spectroscopy (9, 10, 15).

Time-resolved XRD results for the heating (rate 20°C/min) of Cu_2O under a flow of 5%-H_2/95%-He show that the oxide starts to reduce near 300°C and becomes metallic Cu upon further heating (Figure 3a) (10). No intermediate phase is observed during the reduction (i.e. direct transformation
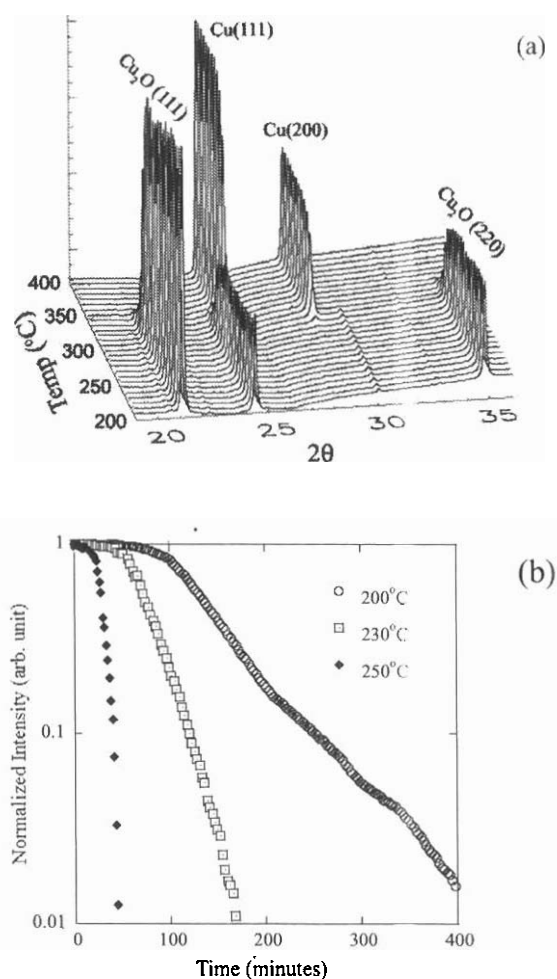
Figure 3. Synchrotron-based   time-resolved *in-situ* XRD patterns (λ= 0.9147Å) taken during the reduction of Cu₂O by H₂ at constant temperature, 250°C (a), and peak intensity plots of the Cu₂O (111) peak as a function of time at different isothermal temperatures (b). The samples were exposed to a 5% H₂/ 95% He gas mixture, 15 ~ 20 cm³/min flow (taken from ref. (10)).

from Cu^{1+} to Cu^0). In these experiments, the desorption of water was detected with a mass spectrometer at temperatures between 300 and 400°C (10). Since the TPR method does not allow a careful determination of the onset temperature for reduction and in some cases makes difficult the generation of intermediate compounds, isothermal reduction experiments were performed. Reduction behaviors at isothermal conditions were similar to the ones determined by TPR means (i.e. no presence of an intermediate phase) (10). In addition, an induction period for reaction was observed as shown in Figure 3b. This figure represents the change for the intensity of the Cu₂O phase as a function of time at isothermal conditions in the temperature range of 200-250°C. The induction period becomes shorter and the reduction rate gets faster when increasing the isothermal temperature: at 230°C, for example, the powder starts to reduce after about 60 minutes and the reduction process completes in 180 minutes, while they are 100 and 450 minutes, respectively, at 200°C. It is worthy to note that ~ 10% of the peak intensity decays during the induction time indicating that a minor reduction already progresses during this period. At this stage, sites are probably being formed that have a high efficiency for the adsorption and dissociation of H₂. Once a large supply of hydrogen is available on/in the oxide sample, the removal of oxygen as water (detected in mass spectroscopy (10)) becomes faster:

$$CuO(solid) + H_2(gas) \rightarrow 2Cu(solid) + H_2O(gas) \quad [1]$$

At the end of the reduction process, the removal of O is difficult. In some cases, not all the Cu₂O completely reduces to a metallic Cu leaving a residue of the starting phase peak even at long exposure to H₂ (>60 minutes). Probably, some Cu₂O grains are coated by a fast reduced Cu film leaving oxygen trapped.

The CuO system exhibits quite interesting behavior during the reduction process (10). First, our TPR results indicate that CuO powder starts to reduce near 280°C under hydrogen flowing, which is slightly (about 20°C) lower than the corresponding
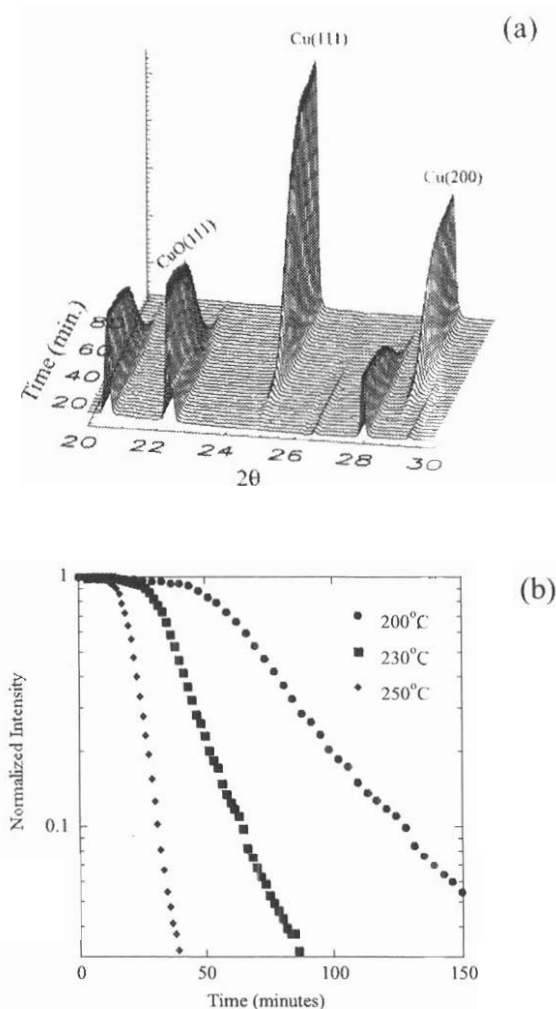
Figure 4. Synchrotron-based   time-resolved *in-situ* XRD patterns (λ= 0.9147Å) taken during the reduction of CuO by H₂ at constant temperature, 200°C (a), and changes of CuO (111) peak intensity as a function of time (b). The samples were exposed to a 5% H₂/ 95% He gas mixture, 15 ~ 20 cm³/min flow (taken from ref. (10)).

temperature found for Cu_2O. Second, time-resolved *in-situ* XRD patterns show that the formation of an intermediate phase depends strongly on the reaction conditions. Under the normal conditions of most

catalytic processes (i.e. substantial pressures of hydrogen), a direct transformation from Cu^{2+} to Cu^0 occurs:

$$CuO(solid) + H_2(gas) \to Cu(solid) + H_2O(gas) \quad [2]$$

As shown in Figure 4a, CuO powders reduce to metallic Cu at 200°C under a 5%-H₂/ 95%-He gas mixture (flow rate >15cc/min) (10). There is no hint of an intermediate phase, Cu_4O_3 or Cu_2O, during the reduction. Instead, diffraction peaks for Cu appear and increase their intensity as the CuO peaks become weaker. A representative plot for the change of peak intensity for the starting CuO phase as a function of time under isothermal conditions (200, 230 and 250°C) is shown in Figure 4b (10). As in the case of Cu_2O reduction, an induction period is seen. The graph shows that the reduction rate becomes slow and the induction period long with decreasing temperature. Figure 5 displays Arrhenius plots for the reduction rates of CuO and Cu_2O. The apparent activation energy of CuO is about 14.5 kcal/mol while the value is 27.4 kcal/mol for Cu_2O (10). Under the conditions of Figures 3 and 4, *the reduction of CuO is easier than the reduction of Cu_2O*. Because of this fact, Cu_2O is probably not seen during the reduction of CuO.

Cu atoms embedded in ceria have an oxidation state higher than those of the cations in Cu_2O or CuO (27). The lattice of the $Ce_{1-x}Cu_xO_2$ systems adopts a fluorite-type structure, but is highly distorted with multiple cation-oxygen distances with respect to the single cation-oxygen bond distance found in pure ceria (Figure 6). Cu approaches the planar geometry characteristic of Cu(II) oxides but with a strongly perturbed local order (27). Figure 7 shows *in situ* time-resolved X-ray diffraction patterns for the reduction (5%H₂/He) and re-oxidation (5%O₂/He) of a $Ce_{0.8}Cu_{0.2}O_2$ sample at 300°C (27). After the reduction process reached its maximum extent, based on the fact that the intensity of metallic Cu became constant, the gas was switched to 5%O₂/He

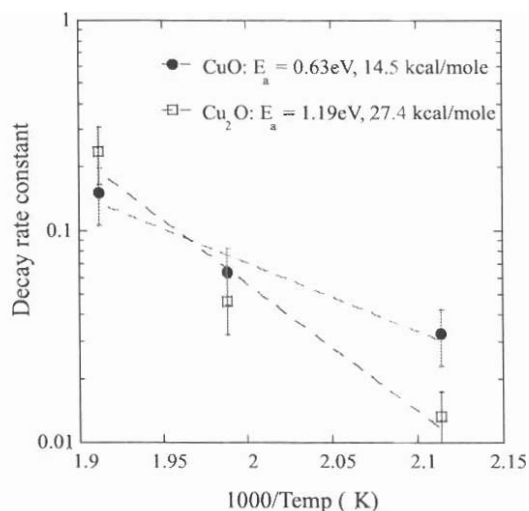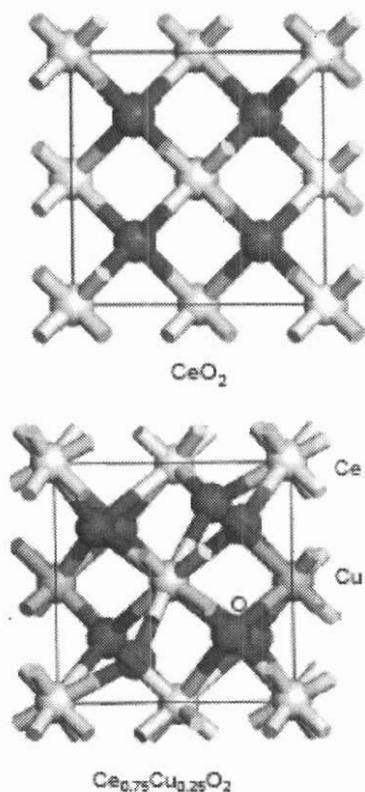Figure 5. Apparent activation energies for the reduction of CuO and Cu₂O (taken from ref. (10)).
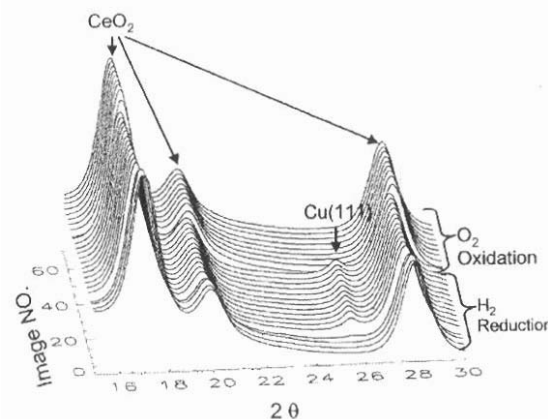

Figure 7. Time-resolved XRD patterns (λ= 0.922Å) for the isothermal reduction (5%H₂/He mixture, flow rate ~ 20cc/minute) and re-oxidation (5%O2/He mixture, flow rate ~ 20cc/minute) of Ce0.8Cu0.2O2 at 300°C (taken from ref (27)).
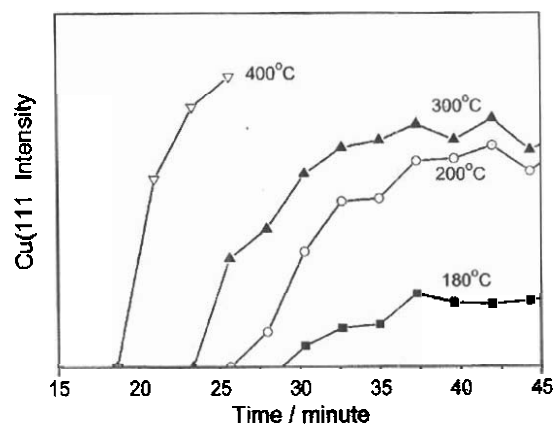

CeO₂

Ce

Cu

Ce₀.₇₅Cu₀.₂₅O₂

Figure 6. Crystal structures for CeO₂ and Ce₀.₇₅Cu₀.₂₅O₂ (taken from ref (27)).

Figure 8. Cu (111) peak intensity in the isothermal reduction of Ce₀.₈Cu₀.₂O₂ at different temperatures with a 5%H₂/He mixture and a flow rate ~ 20cc/minute (taken from ref (27)).

from 5%H₂/He. The metallic Cu disappeared immediately right after the gas switch (this rapid transformation was ob-

served even at a temperature as low as 180°C). However, no CuO or Cu_2O crystalline phase was observed for the reoxidized sample, suggesting that the metallic copper segregated from the $Ce_{0.8}Cu_{0.2}O_2$ during the reduction process was mostly incorporated back into the ceria lattice during reoxidation. Similar XRD results were found for the reduction and reoxidation of $Ce_{0.9}Cu_{0.1}O_2$ and $Ce_{0.95}Cu_{0.05}O_2$ (27).

Figure 8 presents the integrated Cu (111) peak intensities as a function of time for the reduction of $Ce_{0.8}Cu_{0.2}O_2$ in hydrogen at temperatures of 180, 200, 300, and 400°C (27). The isothermal reduction experiments revealed the existence of an induction time, as was detected for the reduction of pure CuO or Cu_2O (10). With a temperature increase, the induction time became shorter. A comparison with the results for CuO reduction in hydrogen under similar reaction conditions (10) indicates that the reduction of the Cu in the doped ceria was slower. The copper atoms in $Ce_{1-x}Cu_xO_2$ were embedded in an oxide lattice that is not easy to reduce (13). In Figure 8, the maximum intensity of the Cu (111) peak depends on the temperature of reduction, demonstrating that the Cu in the doped sample was only partially reduced to metallic Cu, especially at low temperatures. This observation was confirmed by the results of *in situ* X-ray absorption spectroscopy (27).

Previous experiments of H_2-TPR show that the reduction of copper oxide dispersed on other oxides occurs in one, two or even three steps (24) instead of a single step as seen for CuO or Cu_2O (10). These discrepancies could be a consequence of the different conditions used in the reduction experiments, or they could originate from differences in the structural properties of the samples that contain the copper oxide. The time-resolved XRD data for the reaction of H_2 with CuO (10) and $Ce_{1-x}Cu_xO_2$ (24) show substantial variations in the temperature of reduction and in the extent of the reduction process, probably as a consequence of

changes in the structural and electronic properties of the Cu cations.

In Figures 3, 4 and 8, one can see a significant induction time during the reduction of Cu_2O, CuO and $Ce_{1-x}Cu_xO_2$. A similar phenomenon has been detected for the reduction of CuO/CeO_2 (27), NiO (11) and CoMoO4 (26). In the induction period, surface defect sites are created that lead to a high efficiency for the dissociation of H_2 (11). For example, a perfect NiO(100) surface, the most common face of nickel oxide, exhibits a negligible reactivity towards H_2. The presence of O vacancies leads to an increase in the adsorption energy of H_2 and substantially lowers the energy barrier associated with the cleavage of the H-H bond (11). At the same time, adsorbed hydrogen can induce the migration of O vacancies from the bulk to the surface of the oxide (11). A correlation has been observed between the concentration of vacancies in an oxide lattice and the rate of reduction (10, 11, 13, 27).

Water-gas shift reaction on CuO, CuO/CeO_2 and $Ce_{1-x}Cu_xO_2$

A big challenge within the world demand for energy is the need to protect our environment by increasing energy efficiency and through the development of "clean" energy sources. Hydrogen is a potential answer to satisfying many of our energy needs. The water–gas shift (WGS) reaction (CO + $H_2O \rightarrow CO_2 + H_2$) is the main process used in the chemical industry for the production of hydrogen (16). The WGS reaction is usually carried out over catalysts that combine copper and zinc oxides (15, 17) and there is a general desire to improve the performance of this catalytic process. CeO_2-based catalysts have been reported to be very promising for the WGS reaction owing to the peculiar redox properties of ceria and its oxygen storage capacity (28). It is anticipated that, with proper development, CuO-CeO_2 catalysts should realize much higher CO conversions in the WGS than commercial Cu/ZnO catalysts (28, 29). The roles played by the
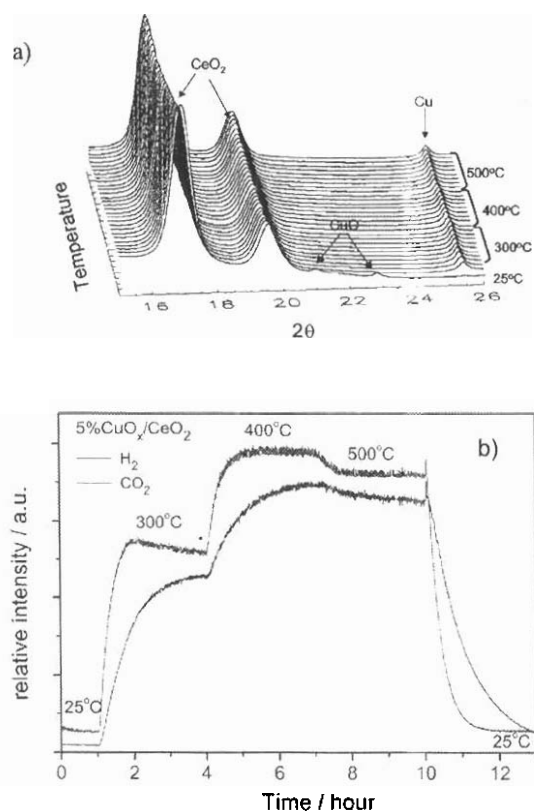
Figure 9.   a) Time-resolved X-ray diffraction patterns for 5%CuOₓ/CeO₂ catalyst during the water gas shift reaction at different temperature ($\lambda = 0.922$ Å). b) The relative concentration of H₂ and CO₂ products as a function of time at different temperatures during the water gas shift reaction as shown in a).

ceria and copper in the WGS over CuO-CeO_2 catalysts are a matter of debate (30). Either metallic Cu or Cu^{+1} cations have been proposed as active sites for the WGS reaction. On the other hand, ceria may not be a simple spectator and play a direct role in the catalytic process. In a recent study, in situ time-resolved XRD was employed to examine the behavior of CuO_x/CeO_2 and $Ce_{1-x}Cu_xO_2$ nanoparticles under different WGS reaction conditions and gas environments (15).

A typical set of time-resolved XRD patterns is shown in Figure 9a for a catalyst that initially contained 5% of CuO_x dispersed on CeO_2 and was exposed to a mixture of CO and H_2O at different temperatures (15). A copper oxide phase was clearly observed at the beginning of experiments at 25°C, and transformed to metallic copper as soon as the temperature was increased to 300°C. By comparing the product curves (Figure 9b) with the XRD patterns, it is clear that the signals for H₂ and CO increase concomitantly with the appearance of metallic copper, indicating the important role of this species during the water gas shift reaction.

The WGS activity of the $Ce_{1-x}Cu_xO_2$ compounds was tested with a methodology similar to that described above for the 5%CuO_x/CeO_2 catalyst (15). The corresponding XRD patterns in Figure 10 indicate that no copper or copper oxides were observed at low temperatures. It must be taken into account in this respect that under these conditions the Cu atoms are more or less uniformly distributed through the bulk and the surface of the ceria particles (27). However, clear features for metallic copper were seen at temperatures above 150°C, and their intensity increased when raising the temperature. This reveals that copper sinters during reduction under WGS conditions in this sample, as shown to occur also under H_2 (27). The mass spectrometer signals for H_2 and CO_2 in Figure 10b show a low WGS activity at temperatures below 220°C, and much higher activity at 300 and 400°C with the presence of metallic copper. Very similar results were found when examining the behavior of a $Ce_{0.95}Cu_{0.05}O_2$ catalyst (15). The results confirmed the important role of metallic copper in the WGS reaction also observed in in-situ XRD results for CuO_x/CeO_2.

Figure 11 compares the production of H_2 during the WGS reaction over the same amount (~5 mg) of CuO, $Ce_{0.8}Cu_{0.2}O_2$, $Ce_{0.95}Cu_{0.05}O_2$ and 5%CuO_x/CeO_2 at different temperatures (15). No activity was observed
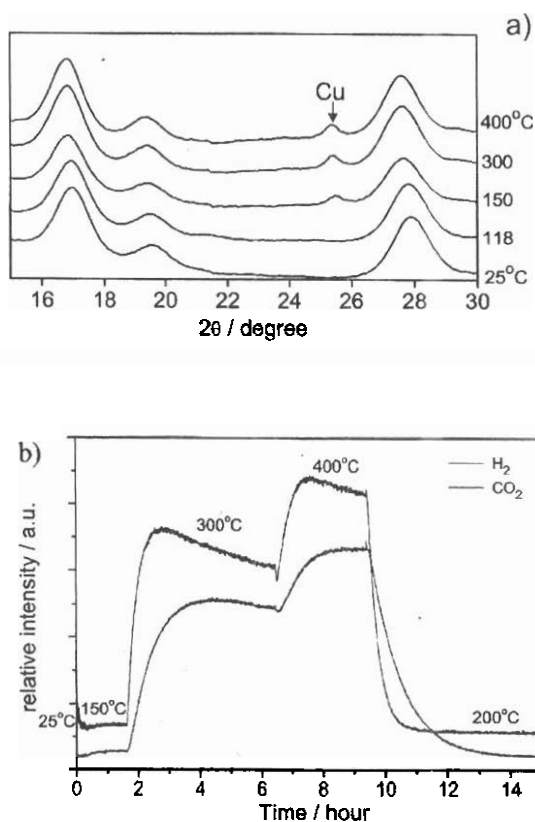
Figure 10. a) Time-resolved X-ray diffraction patterns for $Ce_{0.8}Cu_{0.2}O_2$ catalyst during the water gas shift reaction at different temperature (λ = 0.922 Å). b) The relative concentration of H_2 and CO_2 products as a function of time at different temperatures during the water gas shift reaction as shown in a).

Figure 11. Relative concentrations of H_2 produced from the WGS reaction at different temperatures over $5\%CuO_x/CeO_2$, $Ce_{0.8}Cu_{0.2}O_2$, $Ce_{0.95}Cu_{0.05}O_2$ and CuO with the same operating conditions (Space velocity ~ 1.5×10^5/h).

over pure nano ceria under the present operating conditions. Figure 11 clearly indicates that the impregnated $5\%CuO_x/CeO_2$ sample had better WGS activity than those of doped samples. The catalyst based on pure CuO had little activity. This catalyst certainly had the largest concentration of copper sites among the studied samples. These results indicate that interactions between copper and ceria enhance the activity of the metal in $Cu-CeO_2$ catalysts, suggesting that the WGS
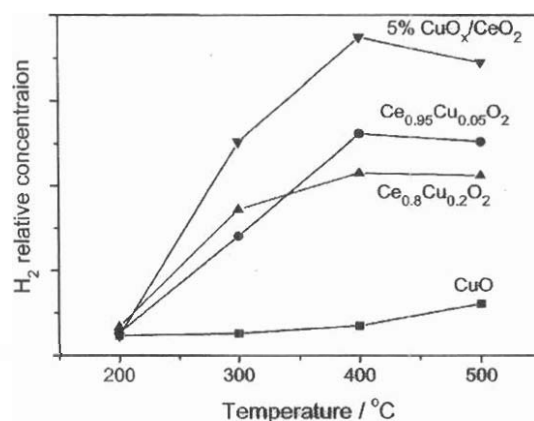
reaction may take place preferentially on the copper/ceria interface [15].

It is well known that oxygen vacancies are easily formed in ceria [17, 27]. Since Ce^{3+} is bigger with respect to Ce^{4+}, a simple reduction leads to a ceria lattice cell expansion [27].

Figure 12 displays the lattice parameters for ceria (Figure 12a) and metallic Cu (Figure 12b) determined from [111] diffraction peaks of time-resolved XRD patterns for $Cu_{0.2}Ce_{0.8}O_2$ under different gases at 300°C. The sample was first heated to 300°C in He and no metallic Cu was observed (Figure 12b). Metallic copper was formed as soon as the gas was switched to 5%CO/He, stayed through the WGS reaction, H_2O exposure, and disappeared after O_2 oxidation. The disappearance of metallic Cu and the practical recovery of the initial lattice parameter in an oxygen environment confirm that the reduction and oxidation of Cu and Ce in $Ce_{0.8}Cu_{0.2}O_2$ is reversible [27]. The lattice of the formed metallic Cu did not change under different gas environments of CO and H_2O. In contrast, the ceria lattice varied significantly (Figure 12a) with an increase after

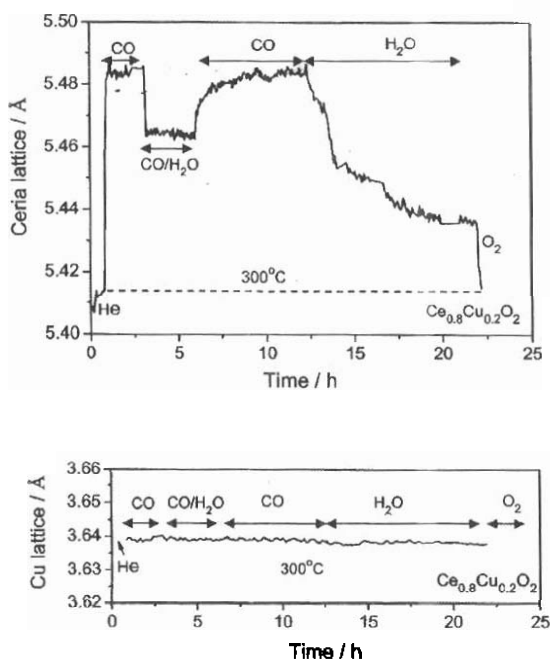Figure 12. Lattice parameters during gas-switch experiments over $Ce_{0.8}Cu_{0.2}O_2$ at 300°C, ceria and b) metallic copper. First the sample was heated in pure He from 25 to 300°C. Then, it was exposed to 5%CO/He, 5%CO/H$_2$O/He, 5%CO/He, H$_2$O/He and 5%O$_2$/He.

exposure to CO and a decrease in H$_2$O, indicating that CO reduced ceria while H$_2$O oxidized it. In other words, CO created oxygen vacancies while H$_2$O eliminated them (15).

Conclusion

The results described above show how powerful can be time-resolved XRD for studying the behavior of heterogeneous catalysts *in-situ* during reaction conditions. The examples discussed are for metal oxide catalysts, but the technique has also been applied successfully to study fluoride, sulfide, carbide and phosphide catalysts (4, 12, 18, 26). Time-resolved XRD can identify the

active phase of a heterogeneous catalyst and how its structure changes after interacting with the reactants and products.

The diffraction studies indicate that, under a normal supply of hydrogen, CuO reduces directly to metallic Cu without formation of an intermediate or suboxide (i.e. no Cu_4O_3 or Cu_2O). The reduction of CuO is easier than the reduction of Cu_2O or $Ce_{1-x}Cu_xO_2$. The reduction of the $Ce_{1-x}Cu_xO_2$ was rather reversible without the generation of a significant amount of CuO or Cu_2O phases during reoxidation. The data of time-resolved XRD for CuO_x/CeO_2 and $Ce_{1-x}Cu_xO_2$ samples indicate that metallic copper and oxygen vacancies in ceria are both involved in the generation of active sites for the production of hydrogen through the water-gas shift reaction.

Acknowledgement

References

1. NORBY P., HANSON J.C. *Catal Today* 39, 301, 1998.

2. THOMAS J.M., GREAVES G.N. *Science* 265, 1675, 1995.

3. CLAUSEN B.S., STEFFENSEN G., FABIUS B., VILLADSEN J., FREIDENHANS R. TOPSOE H. *J Catal* 132 (1991) 524.

4. RODRIGUEZ J.A., CHATURVEDI S., HANSON J.C., BRITO J.L. , *J. Phys, Chem. B*, 103 (1999) 770.

5. RODRIGUEZ J.A., HANSON J.C., CHATURVEDI S., MAITI A., BRITO J.L. *J Chem Phys* 112 (2000) 935.

6. RODRIGUEZ J.A., HANSON J.C., CHATURVEDI S., MAITI A., BRITO J.L. *J Phys Chem B* 104, 8145, 2000.

7. NORBY P., PASHNI F.I., GUALTIERI A.F., HANSON J.C., GREY C.P. *J Phys Chem B* 102, 839, 1998.

8. NORBY P. *J Am Chem Soc* 119 (1997) 5215.

9. WANG X., HANSON J.C., FRENKEL A.I., KIM J.-Y., RODRIGUEZ J.A. *J Phys Chem B* 108, 13667, 2004.

10. KIM J.Y., RODRIGUEZ J.A., HANSON J.C., FRENKEL A., LEE P.L. *J Am Chem Soc* 125, 10684, 2003.

11. RODRIGUEZ J.A., HANSON J.C., FRENKEL A.I., KIM J.Y., PEREZ M. *J Am Chem Soc* 124, 346, 2002.

12. RODRIGUEZ J.A., KIM J.Y., HANSON J.C., SAWHILL S.J., BUSSELL M.E. *J Phys Chem B* 107, 6276, 2003.

13. RODRIGUEZ J.A., WANG X., LIU G., HANSON J.C., HRBEK J., C.H.F. PEDEN, A. IGLESIAS-JUEZ, FERNANDEZ-GARCIA M. *J Molecular Catal A Chemical* 228, 11, 2005.

14. WANG X., RODRIGUEZ J.A., HANSON J.C., PEREZ M. EVANS J. *J Chem Phys* submitted.

15. WANG X., RODRIGUEZ J.A., HANSON J.C., GAMARRA D., MARTINEZ-ARIAS A., FERNANDEZ-GARCIA M. to be published.

16. THOMAS J.M., THOMAS W.J., Principles and Practice of Heterogeneous Catalysis, VCH: New York, 1997.

17. KUNG H.H. Transition Metal Oxides: Surface Chemistry and Catalysis, Elsevier: New York, 1989.

18. CHUPAS P.J., CIRAOLO M.F., HANSON J.C., GREY C. P. *J Am Chem Soc* 123, 1694, 2001.

19. HAMMERSELY A.P., SVENSSON S.O., THOMPSON A. *Nucl Instrum Methods Phys Res* 346, 321, 1994.

20. LARSON A.C., VON DREELE R.B. GSAS General Structure Analysis System. Report

21. LAUR 86-748. Los Alamos National Laboratory: Los Alamos, NM, 1995. (b) H.M. Reitveld, *J Appl Cryst* 2 (1969) 65. c) B.H. Toby. *J Appl Cryst* 34 (2001) 210.

22. DELMON B. in: *Handbook of Heterogeneous Catalysis*, ERTL G., KNöZINGER G.H.,

23. WEITKAMP J. Eds, Wiley-VCH: New York, pp 264-277, 1997.

24. WELLS A.F. *Structural Inorganic Chemistry*. Oxford University Press: New York,

25. 1987.

26. RODRIGUEZ J.A., GOODMAN D.W. *Surf Sci Reports* 14, 1, 1991.

27. SEVERINO F., BRITO J.L., LAINE J., FIERRO J.L.G., LÓPEZ AGUDO A. *J Catal* 177, 82, 1998.

28. NAKAMURA J., CAMPBELL J.M., CAMPBELL C.T. *J Chem Soc Faraday Trans* 86, 2725, 1990.

29. RODRIGUEZ J.A., KIM J.Y., HANSON J.C., BRITO J.L. *Catal Letters* 82, 103, 2002

30. WANG X., RODRÍGUEZ J.A., HANSON J.C., GAMARRA D., MARTINEZ-ARIAS A., FERNANDEZ-GARCIA M. *J Phys Chem B* in press 2005.

31. LI Y. FU Q., FLYTZANI-STEPHANOPOULOS M. *Appl Catal B* 27, 179, 2000.

32. LIU Y.,HAYAKAMA T., SUZUKI K., HAMAKAWA S. *Catal Commun* 2, 195, 2001.

33. BUNLUESIN T., GORTE R., GRAHAM G. *Appl Catal B* 15, 107, 1998.